


## Research Paper

# Use of Porphysomes to detect primary tumour, lymph node metastases, intra-abdominal metastases and as a tool for image-guided lymphadenectomy: proof of concept in endometrial cancer

Lauren Philp<sup>1,2</sup>, Harley Chan<sup>3</sup>, Marjan Rouzbahman<sup>4</sup>, Marta Overchuk<sup>5</sup>, Juan Chen<sup>6</sup>, Gang Zheng<sup>1,5,6,7</sup> and Marcus Q. Bernardini<sup>1,8</sup>

1. Institute of Medical Science, University of Toronto, Toronto, ON, Canada
2. Department of Obstetrics and Gynecology, University of Toronto, Toronto, ON, Canada
3. Guided Therapeutics, TECHNA Institute, University Health Network, Toronto, ON, Canada
4. Department of Pathology, Princess Margaret Cancer Center, University Health Network, Toronto ON, Canada,
5. Institute of Biomaterials and Biomedical Engineering, University of Toronto, Toronto, ON, Canada
6. Princess Margaret Cancer Center, University Health Network, Toronto, ON, Canada
7. Department of Medical Biophysics, University of Toronto, Toronto, ON, Canada
8. Division of Gynecologic Oncology, Princess Margaret Cancer Center, University Health Network, Toronto, ON, Canada

 Corresponding authors: Dr. Lauren Philp, 265 Beatrice Street, Toronto, ON, M6G 3E9. T: 1-647-291-5449; lauren.philp@mail.utoronto.ca. Dr. Gang Zheng gang.zheng@uhnres.utoronto.ca.

© Ivyspring International Publisher. This is an open access article distributed under the terms of the Creative Commons Attribution (CC BY-NC) license (<https://creativecommons.org/licenses/by-nc/4.0/>). See <http://ivyspring.com/terms> for full terms and conditions.

Received: 2018.11.04; Accepted: 2019.02.14; Published: 2019.04.13

## Abstract

**Objective:** To investigate Porphysome fluorescence image-guided resection (PYRO-FGR) for detection of uterine tumour, metastatic lymph nodes and abdominal metastases in a model of endometrial cancer.

**Methods:** White New Zealand rabbits were inoculated with VX2 cells via intra-myometrial injection. At 30 days, Porphysomes were administered intravenously. At 24 h the abdomen was imaged and fluorescent tissue identified (PYRO-FGR). After complete resection of fluorescent tissue, fluorescence-negative lymph nodes and peritoneal biopsies were removed. Histopathology including ultra-staging and analysis by a pathologist was used to detect tumour. Fluorescence signal to background ratio (SBR) was calculated and VX2 (+) tissue compared to VX2 (-) tissue. Biodistribution was calculated and Porphysome accumulation in fluorescent VX2 (+) tissue compared to fluorescent VX2 (-) and non-fluorescent VX2 (-) tissue.

**Results:** Of 17 VX2 models, 10 received 4 mg/kg of Porphysomes and 7 received 1 mg/kg. Seventeen tumours (UT), 81 lymph nodes (LN) and 54 abdominal metastases (AM) were fluorescence-positive and resected. Of these, 17 UT, 60 LN and 45 AM were VX2 (+), while 16 LN and 5 AM were VX2 (-). Nine specimens were excluded from analysis. Thirty-one LN and 53 peritoneal biopsies were fluorescence-negative and resected. Of these, all LN and 51/53 biopsies were VX2 (-) with only 2 false-negative biopsies. Sensitivity and specificity of PYRO-FGR for VX2 (+) tissue was 98.4% / 80.0% overall, 100% / 100% for UT, 100% / 66.0% for LN and 95.7% / 91.4% for AM. Increased SBR and biodistribution was observed in VX2 (+) tissue vs. VX2 (-) tissue.

**Conclusions:** Porphysomes are a highly sensitive imaging agent for intra-operative detection and resection of uterine tumour, metastatic lymph nodes and abdominal metastases.

Key words: Fluorescence guided surgery, Optical Imaging, Porphyrin nanoparticle, Porphysome, Endometrial Cancer

## Introduction

Endometrial cancer is the most common gynecologic malignancy in North America, affecting 2.8% of women throughout their lifetime [1]. Over 95% of patients will have surgical treatment including

a total hysterectomy, bilateral salpingo-oophorectomy and, depending on the risk of lymph node metastases, a pelvic and para-aortic lymphadenectomy, or removal of lymph nodes in the pelvis and

retroperitoneum [2]. Surgical staging to identify lymph node metastases is important as it can guide the administration of adjuvant chemotherapy [3] and radiation [4], and because the presence of lymph node metastases is one of the most important independent prognostic factors for survival [5,6]. While lymphadenectomy is still considered the diagnostic gold standard, significant controversy remains surrounding the procedure. Currently, lymphadenectomy is routinely performed in women with high risk features due to the 18-22% risk of pelvic lymph node metastases [5,7] and the high likelihood of para-aortic lymph node metastases (40-60%) seen with pelvic node positivity [8]. However, this extensive surgical procedure can confer significant associated intra-operative [9] and post-operative morbidity which is related to the extent of lymph node dissection [10]. In low risk women the procedure is controversial, as two large randomized controlled trials have shown that there is no associated survival benefit in this group [9,11]. However, 5-10% of these women will have positive lymph nodes [5,9] that will thus go undiagnosed, preventing them from receiving important adjuvant therapy and confounding their prognosis. Current non-invasive methods to diagnose lymph node metastases including both morphologic (CT, MRI) and functional imaging (PET) do not have the required diagnostic accuracy to replace lymphadenectomy [12], and results from sentinel lymph node studies have been variable, most notably in high risk populations [13,14]. Thus, an improved method of diagnosis and intra-operative targeting of positive lymph nodes is required.

Optical imaging has emerged as a novel technique for cancer diagnosis and treatment by offering a real-time, non-invasive method for tumour detection. Near-infrared fluorescence imaging has emerged as the most clinically important modality [15] given its multiple benefits including safety [16], ease of use [15,17], high resolution and real-time augmentation of the surgical field [15,17]. Furthermore, the decreased background tissue auto-fluorescence [16] and increased depth penetration provides excellent image quality and tissue visualization [16]. As real-time intra-operative fluorescence imaging has allowed surgeons to move seamlessly between pre-operative imaging and intra-operative decision making, the push to develop novel imaging probes has continued. Inorganic molecules such as quantum dots [18], carbon nanotubes [19] and metal nanostructures [20] have rapidly emerged given their optimal fluorescence properties, however concerns regarding toxicity and cost have hampered their translation [21]. Organic fluorophores including next-generation cyanine dyes,

squaraine derivatives, BODIPY analogues and porphyrins/porphyrin derivatives have also been investigated [21], however most require targeting ligand conjugation or nanoparticle encapsulation to improve tumour delivery [21]. Given the significant interest in the development of multifunctional probes for synergistic imaging and therapeutic applications [22], the ability to encapsulate multiple dyes or to perform multi-modal imaging (i.e. PET, MRI) and image-guided therapeutics (i.e. PTT/PDT) with a single particle is desired [19].

To address this clinical need, we have developed the Porphysome [23], an all-organic supramolecular self-assembling nanoparticle (~120 nm diameter), that has unique multi-functionality with respect to cancer imaging and therapeutics [23–26]. After intravenous administration, Porphysomes accumulate preferentially in cancerous tissues due to the abnormal vasculature, microenvironment and increased macrophage population which is known together as the enhanced retention and permeability (EPR) effect. Once in the tumour interstitium, Porphysome nanoparticles dissociate into porphyrin-lipid monomers [23], un-quenching their inherent near-infra fluorescence [23] and allowing for accurate *in vivo* porphyrin fluorescence image-guided resection (PYRO-FGR). Previous studies have demonstrated that intravenous administration of Porphysomes can accurately identify primary tumours, metastatic lymph nodes and micro-metastases using fluorescence in multiple animal models [24–26]. Given this promising pre-clinical data, we hypothesize that Porphysomes could provide a sensitive intra-operative imaging tool to detect primary tumour, lymph node metastases and abdominal metastases using in a model of endometrial cancer. We herein demonstrate the successful use of Porphysomes as a tool for image-guided lymphadenectomy and provide pre-clinical evidence that Porphysomes may be a useful agent to address the clinical controversy regarding the diagnosis and surgical resection of lymph node metastases in endometrial cancer.

## Materials and Methods

### Porphyrin-lipid Nanoparticles

Porphysomes and  $^{64}\text{Cu}$ -labeled Porphysomes were prepared according to previously described protocols including sterile filtration [27] (Figure 1). Briefly, radiolabelling was performed by diluting 0.5 mg/kg of Porphysome solution 1:4 (vol/vol) with 0.1 M  $\text{NH}_4\text{OAc}$  buffer (pH 5.5), mixed with  $^{64}\text{CuCl}_2$  solution, and incubated at 60 °C for 60 min to yield a target activity of 5 mCi per rabbit. The radiolabeling

yield and purity were assessed by instant thin layer chromatography quantified by a Wizard® 1480 well-type automatic gamma counter (PerkinElmer Inc.; Shelton, CT, USA).

## Animal Studies

All animal studies were conducted in Animal Resource Center (ARC) approved facilities of the University Health Network and in accordance with approved animal use and care protocols.

## Establishment of VX2 Endometrial Cancer Model

Two methods were used to prepare cells for intra-myometrial injection. In the first method, *in vivo* VX2 quadriceps tumour propagation was performed as previously described [28]. VX2 tumour blocks from our collaborator's lab were minced into 0.2 mm pieces and strained through a 70 µm cell strainer (Falcon™, Fisher-Scientific) for a final volume of 1 ml and concentration of  $1 \times 10^7$  / ml. In the second novel method, cells were cultured after injecting 150 µL of VX2 cell suspension into the flank of a NOD Scid gamma mouse (Charles River, Wilmington MA, USA). At 34-days the tumour was excised (volume 492 mm<sup>3</sup>) and the non-cystic core was minced onto 60 mm collagen I coated plates (BD/Corning BioCoat). Plates were cultured until adherent cells grew out from tumour pieces at which point cells were cultured on new plates using 1:1 DMEM/F-12 + 10% FBS and 1% Penicillin-streptomycin (Gibco life, ThermoFisher Scientific). After passage 5, DNA was prepared from cell lysates and assayed by qPCR for CRPV- E6, mouse LINE-1 and rabbit LINE-1 to confirm rabbit origin and to assess mouse cell contamination. Cells were frozen in 1:1 DMEM/F-12 + 30% FBS + 10%

DMSO until required at which point they were thawed and cultured according to standard cell culture protocols. The rabbit models developed by these two methods are hereby referred to as *in vivo* rabbits and cultured rabbits respectively.

## 2.1.4 Surgical Protocol and tumour growth monitoring

28 female White New Zealand rabbits weighing 2.5-3.0 kg (Charles River, Wilmington MA, USA) were used for model establishment. After ensuring adequate anesthesia, the peritoneal cavity was entered and the uterine horns were identified and sutured 1.5 cm distal to the cervix using 3-0 Vicryl® suture (Ethicon, Somerville, NJ, USA). 0.5 ml of the cell suspension was injected bilaterally into the myometrium proximal to the suture site. For *in vivo* cells, the injected dose was  $5 \times 10^6$  cells per uterine horn. For cultured cells, the optimal dose was established using an escalating dose protocol with an optimal dose of  $4 \times 10^7$ /ml ( $2 \times 10^7$  per uterine horn) identified. Rabbits were examined for tumour growth at 21 days post-operatively using contrast enhanced CT-imaging and intra-operative assessment with successful tumour growth defined by the presence of a visible/palpable tumour in one or both uterine horns. The timing of the subsequent experiment was based on the type of cell used for model establishment.

## Porphysome Intravenous Injections

Rabbits were separated into low dose (1 mg/kg) and high dose (4 mg/kg) Porphysome groups. For 13 rabbits used for both biodistribution and fluorescence guided surgery experiments, <sup>64</sup>Cu-radiolabelled Porphysomes at a dose of 0.5 mg/kg / 5 mCi were

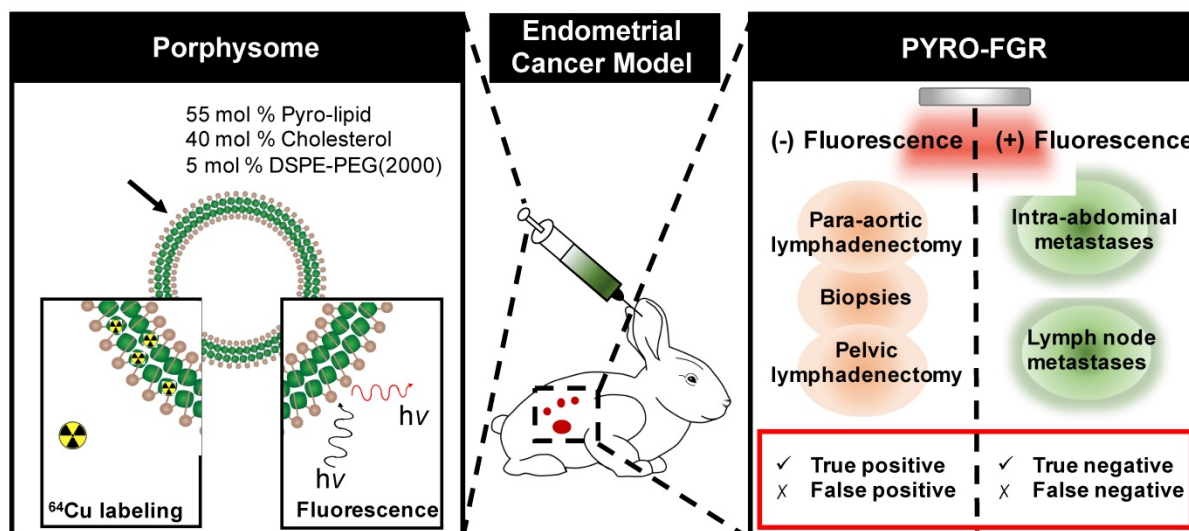


**Figure 1.** Porphysome schematic and the use of porphysomes for porphyrin fluorescence-guided resection (PYRO-FGR). Left panel: schematic representation of the porphysome structure and its functionalities: <sup>64</sup>Cu labeling for PET imaging and gamma counting as well as PYRO-FGR. Right panel: schematics of PYRO-FGR workflow.

intravenously injected with the remaining 0.5 mg/kg (1 mg/kg total) or 3.5 mg/kg (4 mg/kg total) comprised of non-radiolabeled Porphysomes.

### **In vivo near-infrared fluorescence imaging and real-time in vivo porphyrin fluorescence-guided resection (PYRO-FGR)**

At 24 h post-injection, rabbits were euthanized and a systematic white light and fluorescence inspection of the abdomen was performed to identify tumour and intra-abdominal metastatic disease by starting from the uterus and pelvic structures and moving counter-clockwise to examine the pelvic and para-aortic lymph node basins, retro-peritoneal and upper abdominal organs including the diaphragmatic surface and omentum, and the small and large bowel with mesentery. A pre-clinical fluorescence endoscope (PINPOINT imaging system, Novadaq Technologies Inc., Mississauga, ON, Canada) with a laser excitation wavelength of 675 nm was used to for *in vivo* fluorescence imaging and real-time videos were recorded for analysis. All fluorescent tissues were resected under image guidance (PYRO-FGR). Organs with high background fluorescence were not resected unless metastatic nodules were visualized on the organ surface or other suspicious findings were noted (i.e. rough surface, pinpoint bleeding etc.). Once PYRO-FGR was completed, a second systematic white light inspection was performed to identify and resect any remaining non-fluorescent suspicious tissue. Complete pelvic and para-aortic lymphadenectomies and six random biopsies (right and left omental, para-colic gutter and pelvic peritoneum) were then performed after ensuring the tissue was fluorescence negative (Figure 1). All resected tissues were measured and imaged using the Maestro Imaging system™ (Cambridge Research and Instrumentation, Woburn, MA, USA) with a 575 – 645 nm excitation filter and 20 ms exposure. Images were spectrally unmixed and *ex vivo* fluorescence was correlated with *in vivo* fluorescence. Surgery videos were analyzed using Image-J software (public domain software developed by the NIH) and the signal to background fluorescence ratio (SBR) was calculated for each resected tissue by dividing the mean fluorescence signal from the tissue of interest by the mean fluorescence signal of the adjacent background tissue. SBR results were correlated with histology and tumour positive and tumour negative tissues were compared overall and by pyrolipid dose and model type.

### **Biodistribution studies**

In rabbits who received <sup>64</sup>Cu-Porphysomes, half of all primary tumour, lymphadenectomy and biopsy

specimens were used for biodistribution with the remainder sent for histology. 1/3 of the largest intra-abdominal metastases and lymph nodes were used for biodistribution while the remaining 2/3 as well as smaller abdominal metastases and lymph nodes were sent for histology. Additionally, non-tumour bearing organs were also used for biodistribution (Table S1). Specimens were assayed using a Wizard® 1480 well-type automatic gamma counter with a measurement time of 60 s per sample. Results were decay and residual-corrected and the percentage of injected pyrolipid dose per gram of tissue (%ID/g) was calculated. Biodistribution results were correlated with histology and tumour-positive and tumour-negative tissues were compared overall and by pyrolipid dose and model type.

### **Histopathology and ultra-staging protocol**

Non-fluorescent lymphadenectomy specimens and biopsy specimens were serially sectioned (500 µm-1 mm levels) and all sections were stained with Hematoxylin and Eosin (H&E) ± pancytokeratin (M3515 cytokeratin antibody, Dako/Agilent). All fluorescent tissues were frozen in OCT media and after radioactive decay (if applicable) were sectioned and 3 slides 5-10 µm apart were taken at one level: one for H&E staining and one each for pancytokeratin and fluorescence microscopy. Frozen sections were stained with 4',6-Diamidino-2-Phenylindole (DAPI) for nuclei visualization. Full slide fluorescence microscopy was performed on representative tissues using the Zeiss AxioScan.Z1 with Cy5 filter cube (ex 650 nm, em 673 nm, 20 ms) and a DAPI filter (ex. 353 nm, em. 465 nm, 250 ms). All slides were examined by a Gynecologic Pathologist for the presence or absence of tumour. Lymphadenectomy specimens were also examined for negative lymph nodes. Tissues with a negative frozen section underwent an ultra-staging procedure adapted from endometrial cancer sentinel lymph node pathology protocols [29]. Fluorescent tissues were considered negative if they were negative on both frozen section and all ultra-staging sections. Fluorescent tissues were considered positive if they were positive on either frozen section or on any ultra-staging specimen. Specimens were categorized according to tissue type and tumour status: true positives (fluorescent tissue, tumour positive), false positives (fluorescent tissue, tumour negative), true negatives (non-fluorescent tissue, tumour negative) and false negatives (non-fluorescent tissue, tumour positive). Specimens were excluded from analysis if they were not completely assessed intra-operatively (camera malfunction) or post-operatively (unable to perform ultra-staging, presence of cells suspicious for malignancy but not confirmed). The sensitivity and



specificity of PYRO-FGR for primary uterine tumour, lymph nodes and abdominal metastases was then calculated (Figure S1) overall and by pyrolipid dose and model type.

### Statistical analysis

SPSS® (version 24, copyright IBM 2016) was used for statistical analysis. Continuous variables were described using mean values plus standard deviation or standard error of the mean. Continuous variables were compared using two-tailed students-t-test for parametric data and mann-whitney-U tests for non-parametric data. For comparison of multiple means, one-way ANOVA was used with post-hoc Bonferroni correction. A p-value of <0.05 was considered statistically significant.

## Results

### Endometrial Cancer model

21 of 28 rabbits had successful tumour growth. The average time from inoculation to experiment was 29 days (24-31) for *in vivo* rabbits and 45 days (36 - 51) for cultured cell rabbits. Seventeen rabbits were used for PYRO-FGR experiments. One animal died prior to the experiment and three were not used due to equipment malfunction. All rabbits had metastatic transformation of the retroperitoneal lymph nodes with histologically confirmed metastases identified in 16 (one rabbit did not have distinct lymph nodes identified due to the high burden of pelvic disease). Eleven rabbits had histologically confirmed abdominal metastases. 75% of *in vivo* rabbits had  $\geq 1$  metastasis vs. only 40% cultured cell rabbits. One *in vivo* rabbit had distant lung metastases which was not seen in any cultured rabbits. Cultured rabbits had an average of 4.8 lymph nodes removed (2-7) with an average VX2 positivity rate of 79% whereas *in vivo* rabbits had an average of 4 lymph nodes removed (0-9) and 76% positivity. Lymph nodes removed from *in vivo* rabbits were significantly larger and more necrotic when compared to lymph nodes from cultured rabbits with an average volume of 0.99 cm<sup>3</sup> (0.12 - 3.89) vs 0.59 cm<sup>3</sup> (0.01 - 2.92) (p=0.037). *In vivo* rabbits also had larger tumours with an average length 5.6 cm (4 - 6.8 cm) and width of 5.2 cm (3.3 - 9 cm) when compared to cultured rabbits (length 3.6 cm (2-5), width 4.56 cm (3-7)).

Cultured and *in vivo* cell tumours appeared histologically similar with dense hematoxylin stained cells invading muscle and forming glandular structures with many pathological mitotic figures. The cultured VX2 cells were highly positive for both Rabbit LINE-1 and CRPV-E6 with only trace amounts of mouse LINE-1 identified (<0.01 pg/ $\mu$ L).

### *In vivo* porphyrin fluorescence guided resection (PYRO-FGR)

Ten rabbits received 4 mg/kg of Porphysomes (mean volume 10.8 ml (9.3 - 14 ml)) and 7 rabbits received 1 mg/kg (mean volume 2.68 ml (2.4 - 3ml)). In the 4 mg/kg group there were 2 cultured rabbits and 8 *in vivo* rabbits and in the 1 mg/kg group there were 3 cultured rabbits and 4 *in vivo* rabbits. At the 21-day tumour-check laparotomy, all tumours were non-fluorescent and had signal consistent with background uterine tissue.

All tumours, abdominal nodules and lymph nodes resected during PYRO-FGR were intra-operatively fluorescent and discriminated from surrounding background tissue (Videos S1-3). PYRO-FGR allowed for continual reassessment of resection margins which appeared normal in white light (Figure 2). No suspicious tissue was identified on the secondary white light inspection that had not been identified using fluorescence. Subjectively high fluorescence was noted in organs of the reticuloendothelial system, intestines and ovaries (Figure S2). Subjectively low background fluorescence was noted in the non-tumour bearing uterus, bladder, vagina, pelvic and para-aortic lymph node basins, pelvic sidewall muscle, peritoneum and omentum. Rabbits in the low dose group had subjectively lower background fluorescence and off-target tissue fluorescence when compared to the high dose group.

**Table 1.** Histology results by tissue type, Porphysome dose group and VX2 model type

Rabbit Group	Tissue Type										
	Tumour					Lymph nodes					Excluded
	TP	FP	TN	FN	TP	FP	TN	FN	Metastases / Biopsies		
All rabbits (n=17)	17	60	16	31	0	45	5	53	2	12	
1 mg/kg (n=7)	7	29	9	18	0	11	1	33	2	2	
4 mg/kg (n=10)	10	31	7	13	0	34	4	20	0	10	
<i>In vivo</i> cells (n=12)	12	41	11	17	0	41	2	25	1	11	
Cultured cells (n=5)	5	19	5	14	0	4	3	28	1	1	

FN = false negative, FP = false positive, TN = true negative, TP = true positive

Of the 81 fluorescent lymph nodes resected, 60 were VX2 positive, 16 were VX2 negative and 5 were excluded from analysis for previously described reasons. 38% of true positive lymph nodes were diagnosed with ultra-staging and 4 specimens contained only isolated tumour cells. Five of the 16 false positive lymph nodes were removed from a single rabbit. The number of true and false positive lymph nodes in each rabbit group is summarized in Table 1. All 17 uterine tumours resected were intra-operatively fluorescence positive, VX2 positive and considered to be true positive results.

Of the 54 fluorescent abdominal nodules resected, 45 were VX2 positive, 5 were VX2 negative and 4 were excluded from analysis. 29% of true positive nodules were diagnosed with ultra-staging. Of the 5 false positive nodules, 1 contained inflammatory infiltrate and suture material, 3 contained lymphatic tissue and 1 contained no inflammation, suture material or lymphatic tissue.

The number of true positive and false positive abdominal nodules in each rabbit group is summarized in Table 1.

Full-slide fluorescence microscopy of 7 specimens (2 tumours, 2 lymph nodes, 2 abdominal metastases, 1 distant metastasis) demonstrated good correlation between the tumour location and porphyrin fluorescence signal (Figure 3).

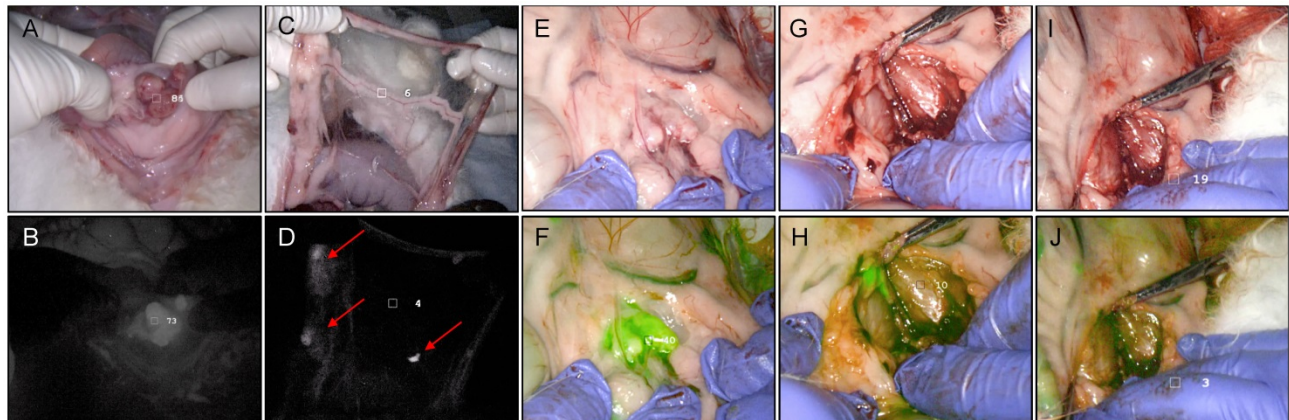


**Figure 2.** *In vivo* porphyrin fluorescence-guided resection (PYRO-FGR), PINPOINT imaging system, 675 nm. (A) Rabbit 11 Tumour, white light. (B) Rabbit 11 Tumour, 675 nm fluorescence grey scale filter. (C) Rabbit 11 Omentum, white light. (D) Rabbit 11 Omentum, 675 nm fluorescence grey scale filter identifying omental metastases (red arrows). (E) Rabbit 9 left pelvic lymph nodes, white light. (F) Rabbit 9 left pelvic lymph nodes, 675 nm fluorescence green filter identifying VX2+ metastatic lymph nodes. (G) Rabbit 9 VX2+ metastatic left pelvic lymph nodes, white light, initial resection. (H) Rabbit 9 VX2 + metastatic left pelvic lymph nodes, 675 nm fluorescence green filter, complete resection demonstrating remaining tumour (bright green). (I) Rabbit 9 VX2 + metastatic left pelvic lymph nodes, white light, complete resection. (J) Rabbit 9 VX2 + metastatic left pelvic lymph nodes, 675 nm fluorescence green filter, complete resection confirmed.

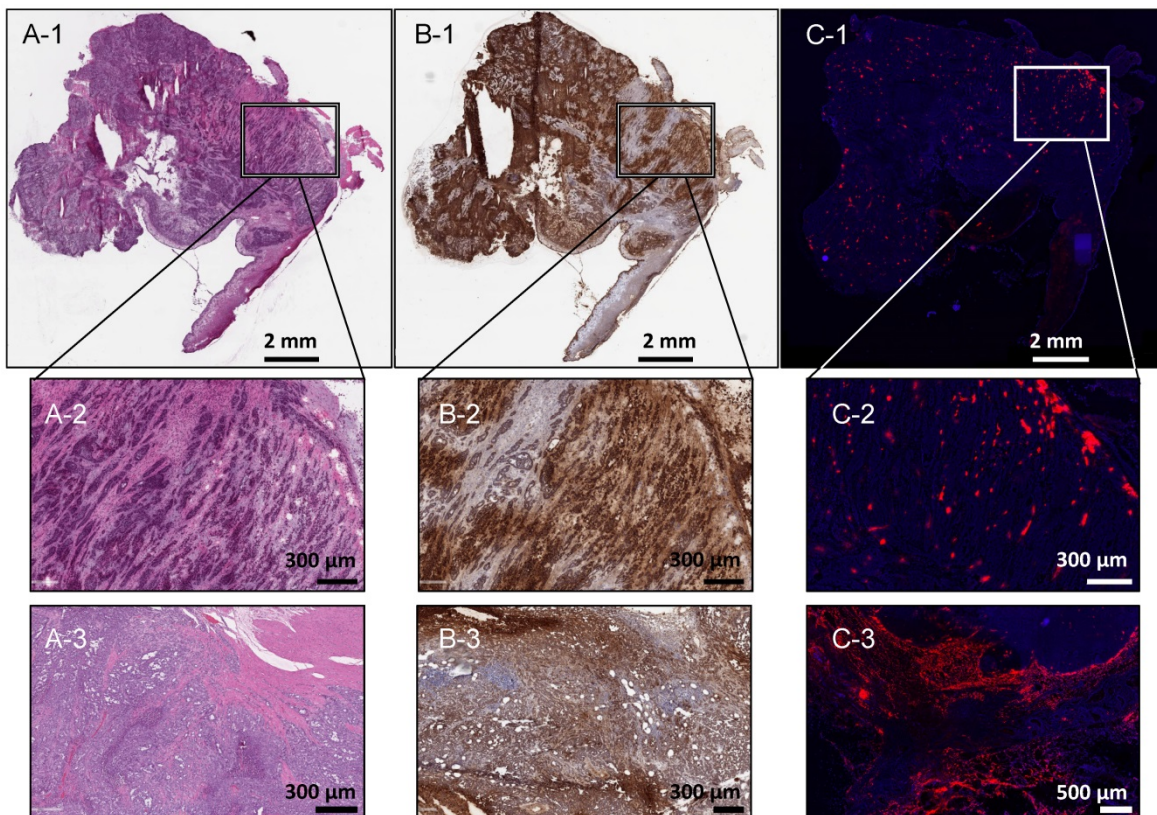


**Figure 3.** Correlation of VX2 uterine tumour location on histopathology and porphyrin signal on fluorescence microscopy. (A-1) Rabbit 24 tumour, 10 µm, H&E, scale 2 mm. (B-1) Rabbit 24 tumour, 10 µm, pancytokeratin staining, scale 2 mm. (C-3) Rabbit 24 tumour, 10 µm, fluorescence microscopy, DAPI (blue, 250 ms), porphyrin (red, 20 ms), scale 2 mm. (A-2) Rabbit 24 tumour, 10 µm, H&E, scale 300 µm. (B-2) Rabbit 24 tumour, 10 µm, pancytokeratin staining, scale 300 µm. (B-3) Rabbit 24 tumour, 10 µm, fluorescence microscopy, DAPI (blue, 250 ms), porphyrin (red, 20 ms), scale 500 µm. (A-3) Rabbit 12 tumour, 10 µm, H&E, scale 300 µm. (B-3) Rabbit 12 tumour, 10 µm, pancytokeratin staining, scale 300 µm. (C-3) Rabbit 12 tumour 10 µm, fluorescence microscopy, DAPI (blue, 250 ms), porphyrin (red, 20 ms), scale 500 µm.



Sixty-four fluorescence-negative lymphadenectomy specimens and 56 biopsies were resected after PYRO-FGR was complete. Twenty-seven lymph nodes were identified within the lymphadenectomies after histologic analysis. Seventeen were from para-aortic lymphadenectomies and 10 from pelvic lymphadenectomies. As well, 4 additional lymph nodes were identified in biopsy specimens for a total of 31 fluorescence-negative lymph nodes, all of which were VX2 negative. The number of true negative lymph nodes in each rabbit group is summarized in Table 1.

Peritoneal biopsies were added to the surgical protocol after the 7<sup>th</sup> rabbit therefore only 10 rabbits had biopsies taken. 53 of 56 were VX2 negative, 2 were VX2 positive and 1 was excluded from analysis. Both false negative biopsies were in the low dose Porphysome group. The number of true negative and false negative biopsies in each rabbit group is summarized in Table 1.

A summary of the sensitivity and specificity of PYRO-FGR for all resected specimens, metastatic lymph nodes and metastatic abdominal nodules is summarized in Table 2. The sensitivity and specificity for primary tumour in all groups was 100% and 100% respectively.

### Signal to background fluorescence ratio

PYRO-FGR videos of 75 lymph nodes, 47 abdominal nodules and 17 tumours were analyzed to

determine the fluorescence signal to background ratio. The signal-to-background fluorescence ratio results by tissue type for each rabbit group is summarized in Figures 4a-4e and the number of specimens per group is summarized in Table S2.

**Table 2.** Sensitivity and specificity of PYRO-FGR for all specimens, metastatic lymph nodes and abdominal metastases by Porphysome dose group and VX2 model type

	Rabbit group	Sensitivity (%)	Specificity (%)
Tissue type resected by PYRO-FGR	All Specimens	98.4	80.0
	1 mg/kg	95.9	83.6
	4 mg/kg	100.0	75.0
	Cultured cells	96.6	84.0
	<i>In vivo</i> cells	98.9	76.4
	Lymph Nodes	100.0	66.0
	1 mg/kg	100.0	66.7
	4 mg/kg	100.0	65.0
	Cultured cells	100.0	73.7
	<i>In vivo</i> cells	100.0	60.7
Intra-abdominal Metastases	All rabbits	95.7	91.4
	1 mg/kg	84.6	97.1
	4 mg/kg	100.0	83.3
	Cultured cells	80.0	90.3
	<i>In vivo</i> cells	97.6	92.6

### Porphysome Biodistribution

13 rabbits received a target radiation dose of 5 mCi (mean 4.54 mCi, (3.25 mCi – 5.72 mCi)) with five receiving a total Porphysome dose of 1 mg/kg and eight receiving a total dose of 4 mg/kg. Three were cultured cell models and 10 were *in vivo* models. The

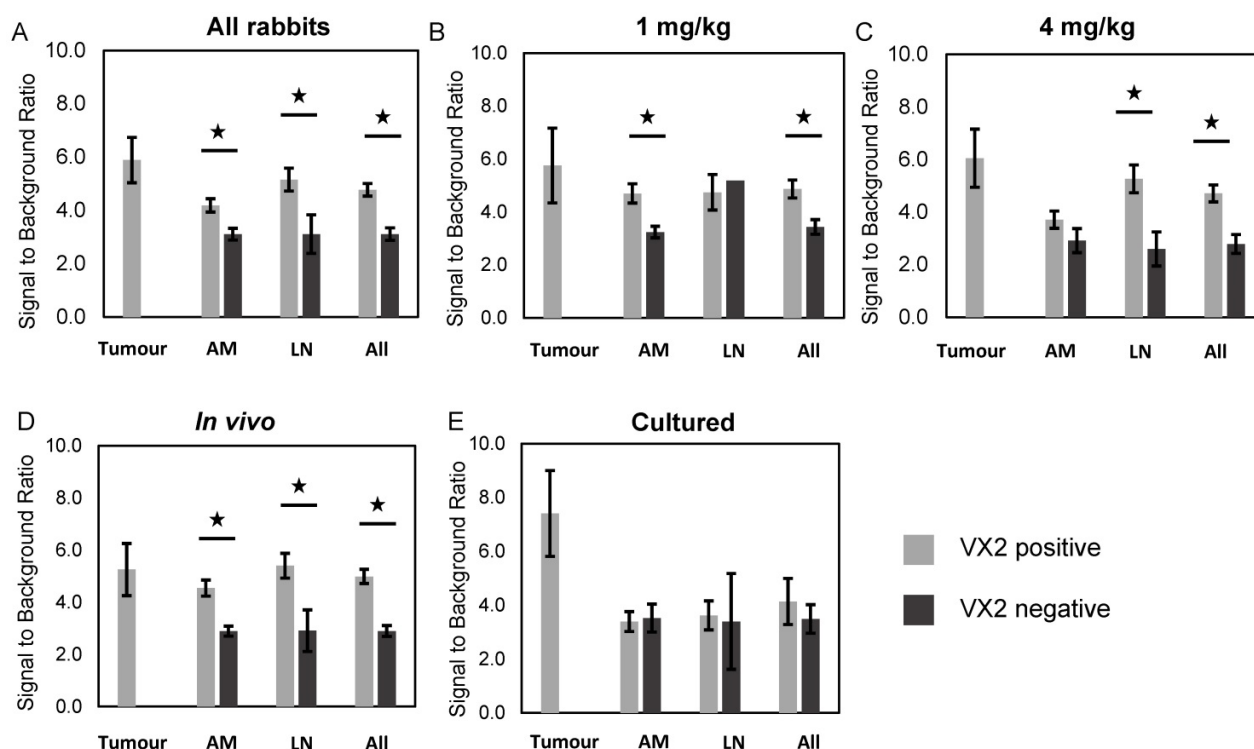


**Figure 4.** Fluorescence signal-to-background ratio, fluorescent VX2 positive vs. fluorescent VX2 negative tissue. (A) All rabbits. (B) 1 mg/kg rabbits. (C) 4 mg/kg rabbits. (D) *in vivo* cell rabbits. (E) Cultured cell rabbits. All = all specimens, AM = abdominal metastases, LN = lymph nodes.

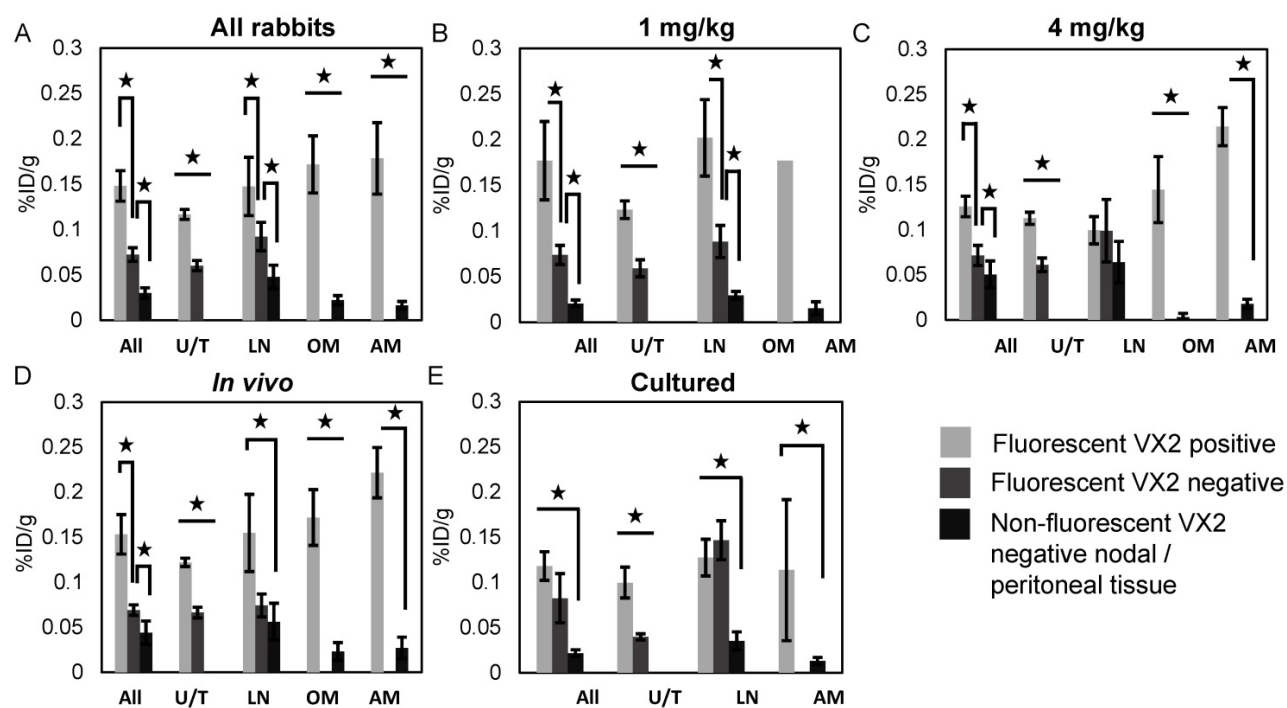


**Figure 5.** Porphysome biodistribution, fluorescent VX2 positive vs. fluorescent VX2 negative and non-fluorescent VX2 negative tissue. (A) All rabbits. (B) 1 mg/kg rabbits. (C) 4 mg/kg rabbits. (D) *in vivo* cell rabbits. (E) Cultured cell rabbits. All = all specimens, AM = abdominal metastases, %ID/g = percent injected dose per gram, LN = lymph nodes, OM = omental metastases, U/T = uterus/tumour.

overall biodistribution data for all tissues in each group is summarized in Figure S3. Thirty-two fluorescent lymph nodes, 9 abdominal nodules, 13 tumours, 15 pelvic and para-aortic lymphadenectomy specimens and 23 biopsies were analyzed. Biodistribution results by tissue type for each rabbit group is summarized in Figures 5a-5e and the number of specimens per group is summarized in Table S3.

## Discussion

We have demonstrated that Porphysomes are a highly sensitive and moderately specific tool for the intra-operative detection of primary tumour, lymph node metastases and abdominal metastases in a rabbit model of endometrial cancer, and that specificity varies by tissue type, cell model type and Porphysome dose. These findings add to the body of evidence surrounding the utility of this multi-modal nanoparticle for cancer imaging and highlights their use as a tool to guide both the detection and real-time resection of metastatic disease.

Current imaging modalities have sensitivities for the diagnosis of lymph node metastases in endometrial cancer that vary widely from 17%-86% [12]. Sensitivities for sentinel lymph node biopsy using interstitial ICG are higher, up to 93% as reported by Plante et al [30], however this procedure is unable to detect distant metastases. The use of intravenous ICG to address the issue of distant metastatic disease has demonstrated variable results

in multiple studies. Veys et al demonstrated only a moderate sensitivity of 72.6% and a specificity of 54.2% for detection peritoneal metastases in ovarian cancer which decreased to 50% for primary ovarian tumours [31]. Studies in metastatic gastrointestinal cancers have demonstrated sensitivities ranging from 76.3% - 87.5% [32,33] however limited conclusions can be drawn due to the lack of rigorous assessment of surrounding peritoneal and gastrointestinal tissues [33]. Xia et al investigated ICG for the detection of metastatic pelvic lymph nodes in prostate cancer but did not report a sensitivity or specificity and notably one false negative lymph node was found in a sample of only four patients [34]. Digonnet et al. reported a higher sensitivity and specificity for metastatic nodes in head and neck cancers of 76.5% and 76.7% respectively which is still lower than our study, however also noted that near-infrared fluorescence imaging may be useful in assessing the margins of resections that appear normal in white light, a finding consistent with our data [35]. Finally, Liberale et al. reported sensitivities and specificities of 51.8 - 77.8% and 75.5 - 94.2% respectively for positive lymph nodes in colorectal cancer however this was based entirely on *ex vivo* analysis [36]. While ICG nanoparticle encapsulation does appear to improve biodistribution and tumour signal to background ratio for image guided surgery, these formulations are still pre-clinical [37,38]. Our reported sensitivity of 100% for tumour and lymph node metastases and



95.7% for abdominal metastases is thus superior to both traditional diagnostic modalities and also to clinically approved intravenously administered near-infrared imaging agents.

This is the first study to report on the sensitivity and specificity of PYRO-FGR and the largest study of Porphysome lymph node imaging to date. Many pre-clinical Porphysome studies in multiple orthotopic cancer models [25,26,39,40] have alluded to this high sensitivity, however, our study was the first to perform a rigorous intra-operative evaluation of both the tissues of interest and surrounding tissues to provide a true evaluation of sensitivity. Our PYRO-FGR surgical protocol, in combination with our meticulous pathology assessment, further ensured the accuracy of our sensitivity assessment. A further strength of our study is the systematic evaluation of sensitivity across multiple tissues types which is also novel in the Porphysome literature. Only two previous studies have looked at the use of Porphysome fluorescence for diagnosis of lymph nodes [25,41] and while both studies evaluated the fluorescence of the first draining lymph node, they did not provide a comprehensive analysis of both positive and negative lymph nodes. This high sensitivity is extremely important with respect to oncologic imaging and is a noted strength of PYRO-FGR, as incomplete tumour resection could result in an increased recurrence risk and compromised oncologic outcomes. The surgical accuracy which can be achieved using PYRO-FGR, most notably with respect to resection tumour margins, is another important finding. As Porphysomes are administered intravenously, the surgical field does not become contaminated with leaking dye which can be problematic with intra-lymphatic imaging agents such as ICG [34], meaning that margin resection can be performed in a highly accurate manner.

Porphysomes were found to be moderately specific, with an increased specificity for uterine tumour and abdominal metastases and a lower specificity for metastatic lymph nodes across all groups, ranging from 60.7 - 73.7%. This moderate specificity in lymph nodes appears to be related to an increased uptake of Porphysomes in negative lymph nodes, resulting in false positive lymph nodes being detected with fluorescence. We hypothesize this may be due to both underlying lymph node tissue characteristics including hyper-vascularity [42] and a large macrophage population [43] but also to an inflammatory response in pelvic lymph nodes from uterine surgical tissue damage [44], necrosis [45] and/or malignancy [46]. Other studies have demonstrated that inflammatory mechanisms such as

an increase in lymphatic flow [47], enlargement and new growth of lymphatic vessels [48] and the recruitment of reactive macrophages due to tumour growth [48] can result in higher nonspecific lymph node accumulation of nanoparticles. Notably, the discrimination of reactive benign and malignant lymph nodes on imaging is a well described challenge as reactive nodes frequently present along the lymphatic drainage pathway of tumours. As well, they can appear enlarged or abnormal on morphologic imaging and as false positive results on functional imaging [44] suggesting this problem is not unique to PYRO-FGR. In comparison, peritoneal tissues are sparsely vascularized, contain fewer organized macrophages [49] and lack a direct lymphatic connection to the tumour site. These characteristics mean peritoneal tissue will have a more subdued inflammatory response and will take up Porphysomes at a lower rate resulting in fewer false positive results. Interestingly, only one false positive abdominal nodule of five in our study did not have a potential reason (i.e. lymphatic tissue or suture material) for fluorescence, suggesting that true false positive abdominal nodules are rare.

Porphysome dose impacted PYRO-FGR specificity in our study. Specificity was highest across all tissues in the 1 mg/kg group when compared to the 4 mg/kg group which may have been related to differences in biodistribution between the groups. A large difference in uptake between true and false positive lymph nodes was noted in the 1 mg/kg group although it is not clear why Porphysomes would accumulate at a proportionally higher rate this group. Potential sources of error include the small number of samples in each group, the small dynamic range (0.1 - 0.25 % ID/g), and variation in tumour volumes across analyzed tissues. This increased biodistribution combined with the decreased background fluorescence from a lower total administered Porphyrin dose likely lead to a higher SBR and improved metastatic tissue discrimination. Unfortunately, due to the auto-gain function of our camera, we cannot quantify the fluorescence signal between groups and thus can comment only on the subjective difference in background fluorescence signal. It is possible that quantification of the difference could eliminate the issues of specificity. As well, no fluorescent lymph nodes were found in healthy control rabbits at 1 mg/kg as compared to those receiving 4 mg/kg. Taken together, these findings suggest that 1 mg/kg may be the optimal PYRO-FGR dose however an even lower dose may further improve discrimination. This is almost certainly true for abdominal metastases, as the 4 mg/kg group contained 80% of all false positive

nodules, and may be true for lymph nodes. However, a dose reduction may increase the risk of false negative results as both false negative biopsies were found in the 1 mg/kg group, although the actual number remained small.

Differences in cell type also impacted specificity. Hyper-vascular, rapidly growing, necrotic tumours such as our *in vivo* tumours have been shown to have more EPR characteristics and higher degrees of tumour associated inflammation when compared to slower-growing tumours such as our cultured cell tumours [50]. These variations in the tumour microenvironment [51] may account for the large differences in Porphysome biodistribution and SBR noted between our model types and we understand that may also be an important factor in future clinical translation, as pre-clinical models do not always reliably replicate the EPR environment of a human tumour. While these differences may have impacted specificity, we hypothesize that our cultured cell model had the best lymph node specificity due to the higher rate of true negative lymph nodes detected in this model. Different tumour growth characteristics meant that metastatic *in vivo* lymph nodes were large and necrotic, leaving little remaining normal lymphadenectomy tissue in which to identify separate negative lymph nodes, whereas metastatic cultured cell lymph nodes were smaller and separated by larger amounts of normal tissue.

This is the first reported use of cultured VX2 cells to create our model and we consider the inclusion of two VX2 cell types to be a strength of our study. The slower growth pattern of our cultured cells is consistent with cultured VX2 cells used for other models [52] and we believe that this growth pattern, in combination with the propensity to form late distant metastases, is an important difference from our *in vivo* model. Human endometrial cancer is generally a slow-growing cancer which generally metastasizes in a stepwise manner from pelvic to para-aortic lymph nodes and finally to late distant metastases. As well, lymph node metastases will generally be separated by normal lymph node tissue. Thus, we consider our novel model to be advantageous as it may replicate the clinical scenario of endometrial cancer more reliably than the more aggressive *in vivo* cells. We realize that the use of two models may act as a confounder during analysis of the dosing group data, just as the two dosing groups may confound the analysis of the model data, however our data was consistent across groups with respect to our hypotheses about Porphysome *in vivo* activity. Unfortunately, given the initial challenges in establishing the cultured cell model, the number of rabbits in the cultured model group is small which

limits the ability to perform sub-group analyses.

Currently, the diagnosis of lymph node metastases in endometrial cancer remains a clinical challenge due to the controversy surrounding the use of lymphadenectomy. We believe that the application of the Porphysome to the problem of endometrial cancer is an innovative way to not only detect cancer in more patients but to improve the treatment of these patients through complete and precise eradication of metastatic disease. Overall, we have demonstrated that Porphysomes are a highly sensitive imaging agent for the detection of primary tumour, metastatic lymph nodes and abdominal metastases in our model of endometrial cancer. The moderate specificity for the detection of metastatic lymph nodes requires improvement, however the identified rates are still be an improvement compared to the current standard of care which removes a majority of unaffected lymph nodes. We are encouraged by the high sensitivity as the resection of false positive tissue is clinically less significant than missing metastatic disease. The issue of decreased specificity is not new in the field of nanotechnology as most nanoparticles rely on a non-specific mechanism for tumour delivery. Given the promising findings in our cultured cell model and our 1 mg/kg dose group, the combination of a lower dose in the environment of a slow-growing tumour may act to improve lymph node specificity while maintaining high specificity for uterine tumour and abdominal metastases. Also, incorporating a quantification system for fluorescence may help eliminate the challenges around sensitivity. Based on this pre-clinical evidence, we believe that Porphysomes could be used as a tool to guide both the intra-operative detection and real-time resection of metastatic lymph nodes in patients with endometrial cancer. Furthermore, we believe that Porphysomes may also have significant utility in other tumours which metastasize throughout the abdomen such as ovarian cancer or gastrointestinal cancers due to the excellent results with respect to primary tumour and abdominal metastatic disease.

## Abbreviations

ANOVA: analysis of variance; CRPV: Cottontail rabbit papillomavirus; CT: Computed tomography; DAPI: 4',6-diamidino-2-phenylindole; DMEM: Dulbecco's modified eagle medium; EPR: Enhanced permeability and retention effect; H&E: Hematoxylin and eosin; %ID/g: Percent injected dose per gram; LINE-1: Long interspersed nuclear element-1; MRI: Magnetic resonance imaging; PDT: Photodynamic therapy; PET: Positron-emission tomography; PTT: Photothermal therapy; PYRO-FGR: Porphyrin fluorescence image-guided resection; qPCR:

Quantitative polymerase chain reaction; SBR: Fluorescence signal-to-background ratio.

## Supplementary Material

Supplementary figures, tables and video legends.  
<http://www.thno.org/v09p2727s1.pdf>

## Acknowledgements

I would like to thank Dr. Marguerite Akens for providing the initial VX2 cells for establishment of the initial VX2 model; Michael Valic and Marta Overchuk for radiolabelling; Dr. Harley Chan for assisted with the surgical establishment of all rabbit models and all fluorescence guided surgery experiments and for analysis of video clips for signal to background ratio calculations; Lili Ding for help with VX2 cell culture and Ariana Rostami and Marco Digrappa for performing the initial VX2 cell culture and PCR analysis; Deborah Scollard and Teesha Komal for help with PET scanning and radiolabelling, Dr. Marjan Rouzbahman for help reading all pathology slides; Napoleon Law for help with pathology; Dr. Juan Chen for help with Porphysome formulation and Dr. Marcus Bernardini and Dr. Gang Zheng for their supervision.

## Funding sources

This study was funded by the Terry Fox Research Institute (PPG#1075), the Canadian Institute of Health Research (Foundation Grant #154326), the Canadian Cancer Society Research Institute (704718), Natural Sciences and Engineering Research Council of Canada, Canada Foundation for Innovation and Princess Margaret Cancer Foundation.

## Competing Interests

The authors have declared that no competing interest exists.

## References

- Canada S. Canadian Cancer Statistics Special topic : Pancreatic cancer. 2017.
- Morice P, Leary A, Creutzberg C, Abu-Rustum N, Darai E. Endometrial cancer. *Lancet*. 2016;387(10023):1094-1108.
- Randall ME, Filiaci VL, Muss H, et al. Randomized phase III trial of whole-abdominal irradiation versus doxorubicin and cisplatin chemotherapy in advanced endometrial carcinoma: A gynecologic oncology group study. *J Clin Oncol*. 2006;24(1):36-44.
- Straughn JM, Huh WK, Orr JW, et al. Stage IC adenocarcinoma of the endometrium: Survival comparisons of surgically staged patients with and without adjuvant radiation therapy. *Gynecol Oncol*. 2003;89(2):295-300.
- Creasman WT, Morrow CP, Bundy BN, Homesley HD, Graham JE, Heller PB. Surgical pathologic spread patterns of endometrial cancer. A Gynecologic Oncology Group Study. *Cancer*. 1987;60(8 Suppl):2035-2041.
- Morrow CP, Bundy BN, Kurman RJ, et al. Relationship between surgical-pathological risk factors and outcome in clinical stage I and II carcinoma of the endometrium: A gynecologic oncology group study. *Gynecol Oncol*. 1991;40(1):55-65.
- Chi DS, Barakat RR, Palayekar MJ, et al. The incidence of pelvic lymph node metastasis by FIGO staging for patients with adequately surgically staged endometrial adenocarcinoma of endometrioid histology. *Int J Gynecol Cancer*. 2008;18(2):269-273.
- Mariani A, Dowdy SC, Cliby WA, et al. Prospective assessment of lymphatic dissemination in endometrial cancer: A paradigm shift in surgical staging. *Gynecol Oncol*. 2008;109(1):11-18.
- ASTEC study group, Kitchener H, Swart A, Qian Q, Amos C, Parmar M. Efficacy of systematic pelvic lymphadenectomy in endometrial cancer (MRC ASTEC trial): a randomised study. *Lancet*. 2009;373:125-126.
- Todo Y, Yamamoto R, Minobe S, et al. Risk factors for postoperative lower-extremity lymphedema in endometrial cancer survivors who had treatment including lymphadenectomy. *Gynecol Oncol*. 2010;119(1):60-64.
- Panici PB, Basile S, Maneschi F, et al. Systematic pelvic lymphadenectomy vs no lymphadenectomy in early-stage endometrial carcinoma: Randomized clinical trial. *J Natl Cancer Inst*. 2008;100(23):1707-1716.
- Haldorsen IS, Salvesen HB. What Is the Best Preoperative Imaging for Endometrial Cancer? *Curr Oncol Rep*. 2016;18(4):1-11.
- Ballester M, Dubernard G, L??curu F, et al. Detection rate and diagnostic accuracy of sentinel-node biopsy in early stage endometrial cancer: A prospective multicentre study (SENTI-ENDO). *Lancet Oncol*. 2011;12(5):469-476.
- Naoura I, Canlorbe G, Bendifallah S, Ballester M, Daraï E. Relevance of sentinel lymph node procedure for patients with high-risk endometrial cancer. *Gynecol Oncol*. 2015;136(1):60-64.
- Wang C, Wang Z, Zhao T, et al. Optical molecular imaging for tumor detection and image-guided surgery. *Biomaterials*. 2018;157:62-75.
- Frangioni J V. In vivo near-infrared fluorescence imaging. *Curr Opin Chem Biol*. 2003;7(5):626-634.
- Vahrmeijer AL, Hutteman M, Van Der Vorst JR, Van De Velde CJH, Frangioni J V. Image-Guided Cancer Surgery Using Near-Infrared Fluorescence. *Nat rev clin oncol*. 2014;10(9):507-518.
- Gao X, Chung LWK, Nie S. Quantum Dots for In Vivo Molecular and Cellular Imaging. *Quantum Dots Appl Biol*. 2007:135-145.
- He X, Gao J, Gambhir S, Cheng Z. Near-infrared fluorescent nanoprobe for cancer molecular imaging: status and challenges. *Trends Mol Med*. 2010;16(12):574-583.
- Xi L, Jiang H. Image-guided surgery using multimodality strategy and molecular probes. *Wiley Interdiscip Rev Nanomedicine Nanobiotechnology*. 2016;8(1):46-60.
- Luo S, Zhang E, Su Y, Cheng T, Shi C. A review of NIR dyes in cancer targeting and imaging. *Biomaterials*. 2011;32(29):7127-7138.
- Huynh E, Zheng G. Engineering multifunctional nanoparticles: All-in-one versus one-for-all. *Wiley Interdiscip Rev Nanomedicine Nanobiotechnology*. 2013;5(3):250-265.
- Lovell JF, Jin CS, Huynh E, et al. Porphysome nanovesicles generated by porphyrin bilayers for use as multimodal biophotonic contrast agents. *Nat Mater*. 2011;10(4):324-332.
- Muhanna N, Cui L, Chan H, et al. Multimodal image-guided surgical and photodynamic interventions in head and neck cancer: From primary tumor to metastatic drainage. *Clin Cancer Res*. 2016;22(4):961-970.
- Muhanna N, Macdonald TD, Chan H, et al. Multimodal Nanoparticle for Primary Tumor Delineation and Lymphatic Metastasis Mapping in a Head-and-Neck Cancer Rabbit Model. *Adv Healthc Mater*. 2015;4(14):2164-2169.
- Liu TW, MacDonald TD, Jin CS, et al. Inherently multimodal nanoparticle-driven tracking and real-time delineation of orthotopic prostate tumors and micrometastases. *ACS Nano*. 2013;7(5):4221-4232.
- Liu TW, MacDonald TD, Shi J, Wilson BC, Zheng G. Intrinsically copper-64-labeled organic nanoparticles as radiotracers. *Angew Chemie - Int Ed*. 2012;51(52):13128-13131.
- Parvinian A, Casadaban LC, Gaba RC. Development, growth, propagation, and angiographic utilization of the rabbit VX2 model of liver cancer: a pictorial primer and "how to" guide. *Diagnostic Interv Radiol*. 2014;20(4):335-340.
- Kim CH, Soslow RA, Park KJ, et al. Pathologic Ultrastaging Improves Micrometastasis Detection in Sentinel Lymph Nodes During Endometrial Cancer Staging. *Int J Gynecol Cancer*. 2013;23(5):964-970.
- Plante M, Touhami O, Trinh X-B, et al. Sentinel node mapping with indocyanine green and endoscopic near-infrared fluorescence imaging in endometrial cancer. A pilot study and review of the literature. *Gynecol Oncol*. 2015;137(3):443-447.
- Veys I, Pop F-C, Vankerckhove S, et al. ICG-fluorescence imaging for detection of peritoneal metastases and residual tumoral scars in locally advanced ovarian cancer: A pilot study. *J Surg Oncol*. 2017;(April 2017):228-235.
- Filippello A, Porcheron J, Klein JP, Cottier M, Barabino G. Affinity of Indocyanine Green in the Detection of Colorectal Peritoneal Carcinomatosis: The Role of Enhanced Permeability and Retention Effect. *Surg Innov*. 2017;24(2):103-108.
- Liberalo G, Vankerckhove S, Gomez Caldon M, et al. Fluorescence imaging after indocyanine green injection for detection of peritoneal metastases in patients undergoing cytoreductive surgery for peritoneal carcinomatosis from colorectal cancer: A pilot study. *Ann Surg*. 2016;264(6):1110-1115.
- Xia L, Zeh R, Mizelle J, et al. Near-infrared Intraoperative Molecular Imaging Can Identify Metastatic Lymph Nodes in Prostate Cancer. *Urology*. 2017;106:133-138.
- Dignonnet A, van Kerckhove S, Moreau M, et al. Near infrared fluorescent imaging after intravenous injection of indocyanine green during neck dissection in patients with head and neck cancer: A feasibility study. *Head Neck*. 2016;1833-1837.



36. Liberale G, Galdon MG, Moreau M, et al. Ex vivo detection of tumoral lymph nodes of colorectal origin with fluorescence imaging after intraoperative intravenous injection of indocyanine green. *J Surg Oncol*. 2016;114(3):348-353.
37. Hill TK, Kelkar SS, Wojtynek NE, et al. Near Infrared Fluorescent Nanoparticles Derived from Hyaluronic Acid Improve Tumor Contrast for Image-Guided Surgery. *Theranostics*. 2016;6(13).
38. Qi B, Crawford AJ, Wojtynek NE, et al. Indocyanine green loaded hyaluronan-derived nanoparticles for fluorescence-enhanced surgical imaging of pancreatic cancer. *Nanomedicine Nanotechnology, Biol Med*. 2018;14(3):769-780.
39. Liu TW, Stewart JM, MacDonald TD, et al. Biologically-targeted detection of primary and micro-metastatic ovarian cancer. *Theranostics*. 2013;3(6):420-427.
40. Jin CS, Wada H, Anayama T, et al. An integrated nanotechnology-enabled transbronchial image-guided intervention strategy for peripheral lung cancer. *Cancer Res*. 2016;76(19):5870-5880.
41. Muhanna N, Jin CS, Huynh E, et al. Phototheranostic porphyrin nanoparticles enable visualization and targeted treatment of head and neck cancer in clinically relevant models. *Theranostics*. 2015;5(12):1428-1443.
42. Gadre A, Briner W, O'leary M. A Scanning Electron Microscope Study of the Human Cervical Lymph Node. *Acta otolaryngologica*. 1994;114(1):87-90.
43. Bellomo A, Gentek R, Bajénoff M, Baratin M. Lymph node macrophages: Scavengers, immune sentinels and trophic effectors. *Cell Immunol*. 2018; 330: 168-74.
44. Liu Y. Postoperative reactive lymphadenitis: A potential cause of false-positive FDG PET/CT. *World J Radiol*. 2014;6(12):890-894.
45. Joris I, Cuénoud HF, Doern G V, Underwood JM, Majno G. Capillary leakage in inflammation. A study by vascular labeling. *Am J Pathol*. 1990;137(6):1353-1363.
46. Claesson-Welsh L. Vascular permeability - The essentials. *Ups J Med Sci*. 2015;120(3):135-143.
47. Ruddell A, Harrell MI, Minoshima S, et al. Dynamic Contrast-Enhanced Magnetic Resonance Imaging of Tumor-Induced Lymph Flow. *Neoplasia*. 2008;10(7):706-IN4.
48. Mumprecht V, Detmar M. Lymphangiogenesis and cancer metastasis. *J Cell Mol Med*. 2009;13(8a):1405-1416.
49. Kumari M, Heeren J, Scheja L. Regulation of immunometabolism in adipose tissue. *Semin Immunopathol*. 2018;40(2):189-202.
50. Danhier F, Feron O, Préat V. To exploit the tumor microenvironment: Passive and active tumor targeting of nanocarriers for anti-cancer drug delivery. *J Control Release*. 2010;148(2):135-146.
51. Prabhakar U, Maeda H, Jain RK, et al. Challenges and key considerations of the enhanced permeability and retention effect for nanomedicine drug delivery in oncology. *Cancer Res*. 2013;73(8):2412-2417.
52. Handal JA, Schulz JF, Florez GB, Kwok SCM, Khurana JS, Samuel SP. Creation of rabbit bone and soft tissue tumor using cultured VX2 cells. *J Surg Res*. 2013;179(1):e127-e132.